WAVELENGTH-DEPENDENT FLUORESCENCE DECAY: AN INVESTIGATION BY MULTIPLE-FREQUENCY PICOSECOND PHASE FLUOROMETRY

J. BAUMANN, G. CALZAFERRI, L. FORSS and TH. HUGENTOBLER

Institute for Inorganic and Physical Chemistry, University of Bern, Freiestrasse 3, CH-3000 Bern 9 (Switzerland)

(Received July 6, 1984; in revised form October 26, 1984)

Summary

Emission-wavelength-dependent fluorescence decay times investigated by multiple-frequency picosecond phase fluorometry are reported for dilute (10^{-5} M) solutions of rhodamine 6G and coumarin 535. In glycerol both dyes show significant wavelength-dependent dual-exponential decay behaviour. In ethanol the decay of coumarin 535 is strictly single exponential with a slightly increasing lifetime towards longer wavelengths. Data have been corrected for the wavelength-dependent photomultiplier transit time difference which is 0.83 ps nm^{-1} for our set-up. The data are described by the kinetics of a two-level system for the excited state. Interpretation is given in terms of different conformations stabilized by glycerol. Rotational diffusion constants are presented for fluorescein, fluorescein ethyl ester and coumarin 535 in ethanol.

1. Introduction

It is known that intramolecular motion influences fluorescence quantum yields of organic dyes in solution [1, 2]. An interesting example, in which the influence of molecular charge transfer on the fluorescence quantum yield has been separated from the influence of intramolecular motion, has recently been discussed by Kosower [3]. In principle we would expect the luminescence decay to depend on this motion because different short-lived conformations might emit preferentially in different regions of the spectrum. Large effects (greater than 1 ns) of decay parameters as a function of the emission wavelength have been reported by several workers [4]. It is not yet clear in which of these cases the various short-lived conformations are involved.

In order to extend the accessible range of this kind of investigation into the picosecond domain we have developed a dual-beam phase fluorometer capable of resolving differences of less than 10 ps in lifetimes of several

0047-2670/85/$3.30

nanoseconds [5 - 8]. In this paper we present the first results for coumarin 535 (1) and rhodamine 6G (2) in glycerol.

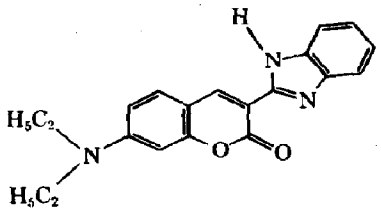

1

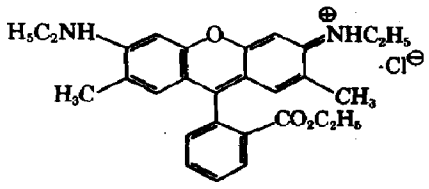

2

To obtain the desired information with the accuracy mentioned above, the wavelength-dependent instrumental response, which in our experiment is predominantly the electron transit time of the photomultiplier, must be eliminated. Systematic errors arise from the observed non-linear sensitivity of our photomultiplier with respect to light intensity even at low levels. We found that the quantum yield of the photomultiplier increases with increasing light intensity over about half the specified dynamic range up to a maximum. This problem is solved by using the variable delay line to calibrate each phase shift measurement against a well-defined geometric displacement.

2. Spectrally resolved lifetimes

Phase shifts for each of the experimental configurations described below were measured at seven different modulation frequencies equally spaced between 20 and 50 MHz. The excitation was at 482.5 nm, the bandpass of the emission monochromator was 4 nm and the temperature was 25 °C. Coumarin 535 (Exciton laser grade) was used as purchased, and rhodamine 6G (Merck) was recrystallized from toluene–ethanol and was purified further by column chromatography. Both dyes were found to be pure by thin layer chromatography. The glycerol and ethanol were Merck Uvasol grade for fluorescence spectroscopy.

Tables 1 and 2 show data for coumarin 535 and rhodamine 6G in glycerol obtained under magic angle polarization conditions. The phase shifts are analysed in terms of single-exponential decay (eqn. (11)) and dual-exponential decay (eqn. (15)) with a_1 fixed at unity. The parameters a_2 and τ_2 are found to be strongly correlated, but τ_1 exhibits almost no correlation with a_2 and τ_2. As a consequence a_2 and τ_2 cannot be determined simultaneously. In order to obtain a comparable estimate of the proportion a_2 of the fast component, τ_2 is assumed to be constant throughout the spectrum. τ_2 can be chosen for both dyes in the interval 50 - 500 ps with very similar values of χ^2. For small τ_2 large coefficients a_2 are found and *vice versa*. However, the changes in the magnitude and sign of a_2 with wavelength are independent of the choice of τ_2. a_2 decreases with increasing wavelength and changes sign at the red edge of the rhodamine 6G emission. In contrast this

TABLE 1

Coumarin 535 (2×10^{-5} mol l^{-1} in glycerol with 0.1% H_2O) observed at magic angle polarization

Wavelength (nm)	*Single-exponential decay*		*Dual-exponential decay*		
	τ (ns)	*Red* χ^2	τ_1 (ns)	a_2	*Red* χ^2
475	2.198	8.95	2.63	2.1	0.15
490	2.242	10.04	2.62	1.7	0.23
505	2.253	10.59	2.50	1.1	0.07
520	2.331	1.14	2.45	0.5	0.24
535	2.399	0.68	2.47	0.3	0.36
550	2.420	0.92	2.47	0.2	0.94
565	2.456	0.88	2.44	−0.1	1.05

$a_1 = 1$; $\tau_2 = 200$ ps; τ_1 is not corrected for self-absorption [9].

TABLE 2

Rhodamine 6G (10^{-5} mol l^{-1} in glycerol with 0.1% H_2O) observed at magic angle polarization

Wavelength (nm)	*Single-exponential decay*		*Dual-exponential decay*		
	τ (ns)	*Red* χ^2	τ_1 (ns)	a_2	*Red* χ^2
535	2.816	15.2	3.58	3.1	0.30
550	3.386	8.55	3.66	0.9	0.45
565	3.895	1.02	3.79	−0.3	0.34
580	4.110	3.28	3.86	−0.8	0.70

$a_1 = 1$; $\tau_2 = 200$ ps; τ_1 is not corrected for self-absorption [9].

region is described well by a single exponential for coumarin 535. The slow component τ_1 decreases with emission wavelength for coumarin 535 but increases for rhodamine 6G. Malley and Mourou [10] have shown that the emission spectrum of rhodamine 6G in glycerol shifts to longer wavelengths during the first 100 ps after excitation and changes its shape. Their results are consistent with our observation of a fast decay τ_2 which we fixed at 200 ps for our data analysis and whose physical interpretation will be given in Section 3.

Table 3 shows the lifetimes of coumarin 535 in ethanol. The decay is excellently described across the whole spectrum by a single lifetime which increases slightly at longer wavelengths.

It is of interest for some applications to note that rotational relaxation constants can be obtained with the dual-beam modulation technique using two independent experimental arrangements: phase shift between the sample (parallel or perpendicular polarization) and a scatterer (eqn. (22)); phase shift between parallel emission and perpendicular emission from the sample (eqn. (23)). The rotational relaxation constants of three dyes in ethanolic

TABLE 3

Degassed coumarin 535 solution (10^{-5} mol l^{-1} in ethanol with 5% H_2O) observed at magic angle polarization

Wavelength (nm)	*Single-exponential decay*	
	τ (ns)	*Red* χ^2
475	2.764 ∓ 0.006	0.36
490	2.770 ∓ 0.007	0.26
505	2.772 ∓ 0.004	0.23
520	2.775 ∓ 0.006	0.13
535	2.794 ∓ 0.006	0.08
550	2.808 ∓ 0.009	0.37

τ is not corrected for self-absorption [9].

TABLE 4

Rotational relaxation constants of fluorescein, fluorescein ethyl ester and coumarin 535 (10^{-5} mol l^{-1} each) in ethanolic solution

Dye	*Solvent*	*Emission wavelength* (nm)	τ (ns)	τ_{rot} (ps)
Fluorescein	95% ethanol 5% H_2O 10^{-3} M NaOH	535	4.126 ± 0.007	306 ± 2
Fluorescein ethyl ester	95% ethanol 5% H_2O 10^{-3} M NaOH	535	4.441 ± 0.008	227 ± 2
Coumarin 535	95% ethanol 5% water	505	2.772 ± 0.004	174 ± 2
		535	2.794 ± 0.006	172 ± 4

τ is not corrected for self-absorption [9].

solution determined by the second method are presented in Table 4 together with the lifetimes τ; the rotation is assumed to be spherical.

3. Kinetic scheme and quantum-chemical picture

The behaviour observed for rhodamine 6G and coumarin 535 in glycerol is inconsistent with a simple Jablonski diagram. We introduce a two-level scheme for the excited state (Fig. 1) in order to obtain agreement with our data. The response of this system to an exciting δ pulse is described by

$$\frac{dL_1}{dt} = -(k_1 + k_{12})L_1 + k_{21}L_2$$

$$\frac{dL_2}{dt} = k_{12}L_1 - (k_2 + k_{21})L_2 \qquad (1)$$

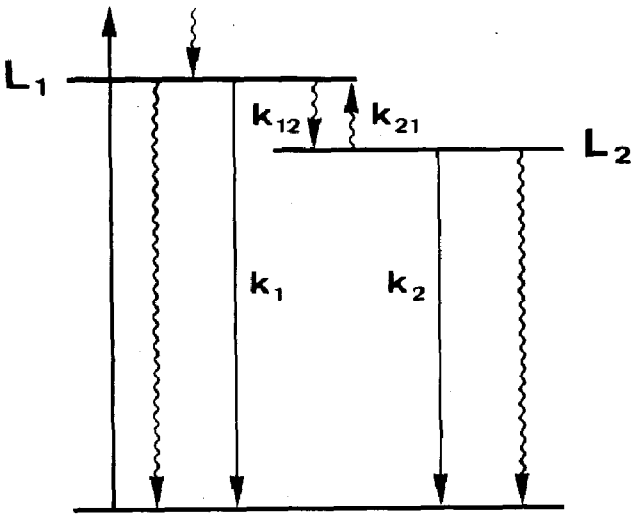

Fig. 1. Two-level scheme.

The radiationless decay and intersystem crossing are not explicitly included because they only lead to an additive factor in k_1 and k_2. This model requires four rate constants, but our data only allow the introduction of two rate constants in those regions which cannot be described by a single-exponential decay. The most reasonable simplification is to neglect $k_{21}L_2$. In this case eqn. (1) becomes

$$L_1(t) = L_1(0)\exp\{-(k_1 + k_{12})t\}$$
$$L_2(t) = L_1(0)\frac{k_{12}}{k_1 - k_2 + k_{12}}[\exp(-k_2 t) - \exp\{-(k_1 + k_{12})t\}] \quad (2)$$

Figure 1 must be interpreted in such a way that the observed emission $I_{em}(t)$ is composed of two contributions:

$$I_{em}(t, \lambda) = q(\lambda)L_1(t) + r(\lambda)L_2(t) \quad (3)$$

$q(\lambda)$ and $r(\lambda)$ describe the shape of the two subspectra. According to Fig. 1 the spectrum $r(\lambda)$ will be red shifted with respect to $q(\lambda)$. Inserting expression (3) into eqn. (2) leads to

$$I_{em}(t, \lambda) = L_1(0)\left[\left\{q(\lambda) - r(\lambda)\frac{k_{12}}{k_1 - k_2 + k_{12}}\right\}\exp\{-(k_1 + k_{12})t\} + \right.$$
$$\left. + r(\lambda)\frac{k_{12}}{k_1 - k_2 + k_{12}}\exp(-k_2 t)\right] \quad (4)$$

The interpretation of the rate constants in terms of luminescence decay times is given by

$$\tau_1 = \frac{1}{k_2} \qquad \tau_2 = \frac{1}{k_1 + k_{12}} \quad (5)$$

It is easier to discuss the physical meaning of eqn. (4) if we assume that $k_1 \approx k_2$. In this case we obtain

$$I_{em}(t, \lambda) = L_1(0)\left[\{q(\lambda) - r(\lambda)\} \exp\left(-\frac{t}{\tau_2}\right) + r(\lambda) \exp\left(-\frac{t}{\tau_1}\right)\right] \quad (6)$$

It is obvious that $q - r > 0$ corresponds to the short-wavelength region, $q = r$ leads to single-exponential behaviour and $q - r < 0$ corresponds to the long-wavelength region. If we now look at Table 1 where the wavelength-dependent decay parameters of coumarin 535 in glycerol are reported, we can see that up to 535 nm these data are consistent with the short-wavelength region of expressions (4) and (6). In view of the difficulty in determining τ_2 from the data a reasonable order-of-magnitude estimate for k_{12} is 10^{10} s^{-1}.

Single-exponential behaviour is observed at 550 and 565 nm. In ethanol (see Table 3) coumarin 535 shows single-exponential behaviour over the whole wavelength region. Consequently k_{12} in this solvent must be much larger than k_{12} in glycerol. The slightly increasing lifetime may be the result of the presence of this very fast decay component which cannot be resolved at present.

It is interesting to note that in the case of rhodamine 6G we can observe the region with $q - r < 0$ as well; this provides strong evidence that level 2 is populated from level 1. However, the significant wavelength dependence of τ_1 for rhodamine 6G and coumarin 535, which cannot be explained by this kinetic scheme, still remains. It would be consistent with our observations to assume that many, rather than one, L_2 levels exist, each with a slightly different decay time.

In order to obtain a better idea of what such a two-level system could mean, we apply simple quantum-mechanical arguments. Some years ago we described the influence of intramolecular motion on the fluorescence quantum yield of organic dyes in solution [1]. Since then our description has turned out to be consistent with many new results reported in the literature [2, 3]. Other mechanisms exist for fast intramolecular relaxation, *e.g.* solvent effects due to intramolecular charge transfer in the first excited singlet state [3, 11] or specific intramolecular interactions which will be discussed below. However, in the absence of intersystem crossing, the same question always requires an answer: How is the electronic energy transferred into vibrational energy? In ref. 1 we proposed that σ–π interactions due to out-of-plane intramolecular motion were responsible for fast thermal relaxation because the σ framework strongly couples with the vibrations. There are many different decay times in isolated molecules because the Franck–Condon factors for each pair of vibrational levels (ν_u, ν_l) are generally different. Most of this detailed structure is not observed in solution because of the fast vibrational relaxation due to molecule–solvent interactions. However, we would still expect different conformations to have slightly different decay times, provided that their thermal depopulation is not too fast. Solvent interactions can stabilize some of them. In addition we can ask

whether specific intramolecular interactions could stabilize excited state conformations. This could lead to different lifetimes for different conformations. At this point it is necessary to remember that the lactone forms of rhodamine 110 and fluorescein are stable in aprotic solvents [11]. We have observed that fluorescein and fluorescein ethyl ester in alkaline ethanolic solution (10^{-3} M NaOH) and rhodamine 110 in acid ethanolic solution (10^{-3} M HCl) are stable under irradiation with light of 482.5 nm (approximately 100 mW mm^{-2}), but that bleaching can be observed easily in glycerol solutions under the same conditions. We have not analysed the photoproducts, but it is possible that lactone is formed. Another possibility is the photoreduction of the dye and oxidation of the solvent. This photoreaction appears to be reversible on a time scale of a few seconds for fluorescein and fluorescein ethyl ester, but it is irreversible for rhodamine 110. It is interesting to note that sulphorhodamine 101, which is stable in ethanol, shows the same type of instability in glycerol, whereas rhodamine 6G and coumarin 535 are stable under the same conditions. We shall consider whether a mechanism which could lead to lactone formation in fluorescein and rhodamine 110 might be responsible for the complicated decay kinetics of rhodamine 6G. Such a mechanism could be regarded as a combination of the intramolecular motion described in ref. 1 and a specific intramolecular two-centre interaction. We have checked whether extended Hückel molecular orbital (EHMO) calculations with the parametrization given by Hoffmann and coworkers [12] are capable of describing the first two singlet–singlet transitions of dyes such as rhodamine 110, fluorescein, methincyanine, various coumarin dyes and thionine, and we have found that this simple method is more useful than the Pariser–Parr–Pople (PPP) method [13] for our type of problem. This is because the σ framework is included in EHMO calculations. It is interesting that the accidental degeneracy which is observed in ZDO calculations on naphthalene and which is a textbook example for configuration interaction [14] disappears as soon as overlap integrals are introduced but to get the $^1B_{3u}$ state below the $^1B_{2u}$ state configuration interaction is still necessary. The following arguments are based on this type of calculation.

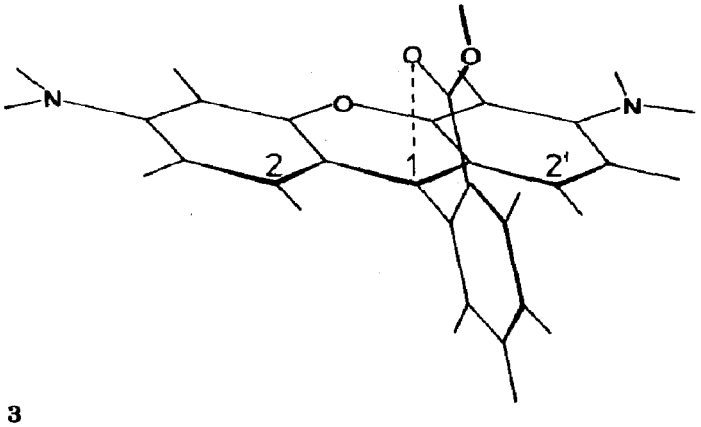

3

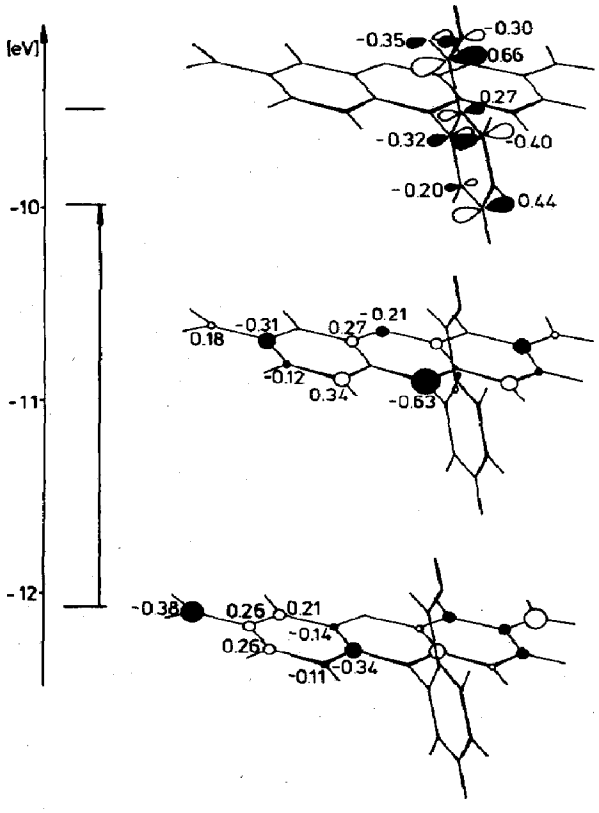

Fig. 2. Frontier orbitals for rhodamine 110. The phenyl group is orthogonal to the chromophore.

The most important frontier orbitals for rhodamine 110 (3) with a phenyl group twisting angle of 90° are shown in Fig. 2. Calculations have also been carried out for a twisting angle of 75°. The orbital energies at both angles are very similar, but the energy difference between the highest occupied molecular orbital (HOMO) and the lowest unoccupied molecular orbital (LUMO) at 75° is slightly smaller than that at 90° indicating that different conformations might correspond to different regions in the emission spectrum. The calculated orbital coefficients [14, 15] are also indicated. From these results we can see that absolutely no charge is transferred to the phenyl group at 90° in the $S_1 \leftarrow S_0$ transition. Some charge redistribution on the orbitals indicated occurs at 75° and this becomes more pronounced at smaller angles. Small angles seem to be less important because of large steric interactions. When an electron is excited from HOMO to LUMO the most important change occurs at the carbon atoms 1, 2 and 2′. Application of second-order perturbation theory shows that the interaction energy ΔE between an atom r and an atom s arising from an unoccupied orbital u and an occupied orbital o is given by [16]

$$\Delta E = \frac{n(C_r C_s \beta_{rs})^2}{\epsilon_u - \epsilon_o} \tag{7}$$

where n indicates the number of electrons involved. In the EHMO description β is proportional to the overlap integral. In view of the results reported in Fig. 2 we do not expect any significant interaction between the carboxyl oxygen and the carbon atoms 1, 2 and 2′ with respect to the HOMOs and LUMOs. However, inspection of the $2\pi^*$ orbital reveals that significant $1\pi^*-2\pi^*$ interaction in the first excited state is possible. This interaction could be responsible for photochemically induced lactone formation provided that the overlap integral is non-zero.

The energy of the $2\pi^*-1\pi^*$ interaction between the carboxyl oxygen and the carbon atom in position 1 estimated from eqn. (7) is 0.0 kJ mol^{-1} for the carbon atom at 90° to the carboxyl group and the carboxyl group in the same plane as the phenyl group position. This result is expected from symmetry arguments. At 75° the interaction energy is approximately 1 kJ mol^{-1}. Small changes in bond angles and bond lengths allow stronger interactions. From this result we conclude that the hypothesis that a specific intramolecular interaction might be responsible for the existence of excited state conformations with sufficiently long lifetimes to lead to wavelength-dependent luminescence decay times is consistent with a molecular orbital picture. The lifetime of individual conformations is expected to increase with increasing viscosity of the surroundings. The description presented is highly speculative. Nevertheless, it may help in the development of more specific ideas concerning the influence of various conformations and intramolecular interactions on the relaxation behaviour of molecules in solution.

The frontier orbitals of coumarin 535 for a planar conformation and a conformation twisted at an angle of 90° are shown in Fig. 3. The planar conformation is found to be 43 kJ mol^{-1} less stable than the twisted conformation in the ground state. In the first excited state the planar conformation is stabilized as can be seen from the molecular orbital diagram, and some charge redistribution occurs which is different from that sometimes reported in the literature [17]. Full rotation in the nanosecond time scale is therefore unlikely in either the ground or the first excited state.

4. Data analysis

The basic theory for data analysis in modulation experiments is well known [18, 19]. For our dual-beam experiment some special equations have to be derived and some simplifications are possible. In this section we describe the equations needed for multiexponential decay analysis and for rotational diffusion of a sphere. It is sometimes implied in the literature that the derivation of the equations for modulation experiments is complicated. This is not the case because if the impulse response is derived in real time the equations in frequency space can be obtained by Fourier transformation.

The experimental phase shift Φ_{exp} is composed of various contributions from which the part due to the radiative lifetime of the sample can be

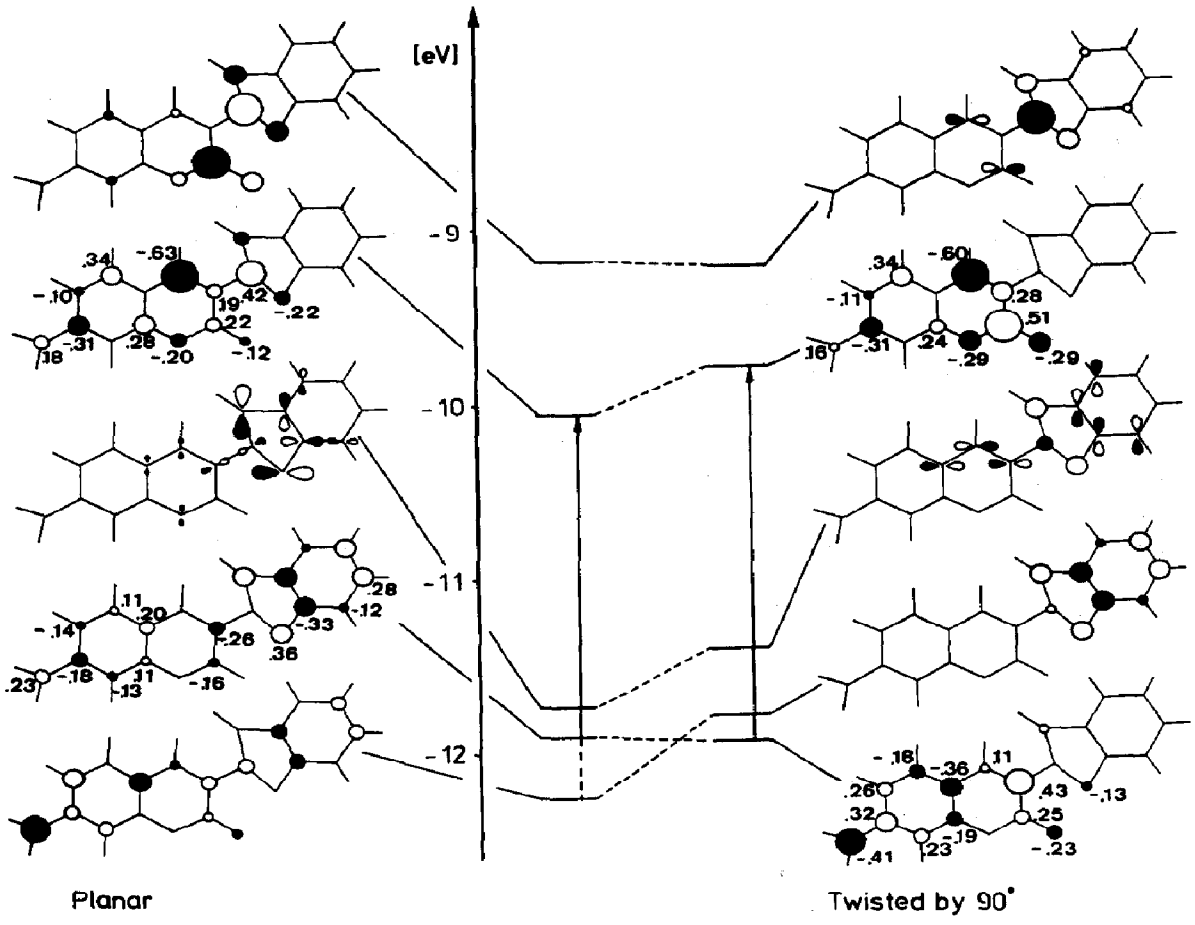

Fig. 3. Frontier orbitals for coumarin 535 for the planar conformation and the conformation twisted at an angle of 90°. The orbital coefficients for the π (HOMO) and the π (LUMO) are indicated.

determined in our experiments with an accuracy to approximately 1 mrad [6 - 8]. This phase shift has to be compared with the theoretical phase shift Φ_{th} calculated from the assumed decay model.

The phase shift due to luminescence decay is described by

$$\tan \Phi_{th} = f(\tau_1, \tau_2, \ldots, \tau_n; a_1, a_2, \ldots, a_n; \omega) \tag{8}$$

In our dual-beam modulation experiment Φ_{exp} is always the phase difference between the modulated luminescence from a sample S and a reference R. The quantity to be compared with the experiment is therefore

$$\tan \Phi_{th} = \tan(\Phi_S - \Phi_R) = \frac{\tan \Phi_S - \tan \Phi_R}{1 + \tan \Phi_S \tan \Phi_R} \tag{9}$$

If the reference cell contains a scatterer eqn. (9) reduces to

$$\tan \Phi_{th} = \tan \Phi_S \tag{10}$$

The parameters τ_i and a_i in eqn. (8) are obtained from a least-squares procedure which establishes the best match between $\Phi_{exp}(\omega)$ and $\Phi_{th}(\omega)$.

The impulse response of a single-exponential decay without rotational diffusion is given by [18]

$$T(t) = \frac{1}{\tau} \exp\left(-\frac{t}{\tau}\right) \tag{11}$$

In modulation experiments we observe a phase shift related to the Fourier transform of this function:

$$T(\omega) = \frac{1}{\tau} \int_0^\infty \exp\left(-\frac{t}{\tau_e} - j\omega t\right) dt = \frac{1}{1 + j\omega\tau} \tag{12}$$

It is convenient to split $T(\omega)$ into its real and imaginary parts

$$T(\omega) = \frac{1}{1 + \omega^2\tau^2} - j\frac{\omega\tau}{1 + \omega^2\tau^2} \tag{13}$$

because the tangent of the phase shift is equal to the absolute value of the ratio of the imaginary part to the real part:

$$\tan \Phi = \omega\tau$$

or

$$\tan(\Phi_S - \Phi_R) = \omega \frac{\tau_S - \tau_R}{1 + \omega^2\tau_S\tau_R} \tag{14}$$

The impulse response for a multiexponential function is

$$T(t) = \frac{1}{\Sigma_i a_i\tau_i} \sum_i a_i \exp\left(-\frac{t}{\tau_i}\right) \tag{15a}$$

from which we easily obtain the Fourier transform

$$T(\omega) = \frac{\Sigma_i a_i\tau_i/(1 + \omega^2\tau_i^2)}{\Sigma_i a_i\tau_i} - j\frac{\Sigma_i a_i\omega\tau_i^2/(1 + \omega^2\tau_i^2)}{\Sigma_i a_i\tau_i} \tag{15b}$$

It is very convenient that the weighting factor $\Sigma_i a_i\tau_i$ disappears in the expression for $\tan \Phi$:

$$\tan \Phi = \omega \frac{\Sigma_i a_i\tau_i^2/(1 + \omega^2\tau_i^2)}{\Sigma_i a_i\tau_i/(1 + \omega^2\tau_i^2)} = \omega \frac{Z}{N} \tag{16}$$

Inserting eqn. (16) into eqn. (9) yields

$$\tan(\Phi_S - \Phi_R) = \omega \frac{Z_S N_R - Z_R N_S}{N_S N_R + \omega^2 Z_S Z_R} \tag{17}$$

Z_p and N_p ($p \equiv$ S, R) are defined by

$$Z_p = \sum_i (a_p)_i \frac{(\tau_p^2)_i}{1 + \omega^2(\tau_p^2)_i}$$

$$N_p = \sum_i (a_p)_i \frac{(\tau_p)_i}{1 + \omega^2(\tau_p^2)_i}$$

The following two equations, which are derived from eqn. (16), are convenient for dual-exponential decay in the absence of rotational diffusion or when observed at the magic angle [20].

(1) Both the reference and the sample contain a dye which exhibits dual-exponential decay:

$$\begin{aligned} N_p &= a_{p_1}\tau_{p_1}(1 + \omega^2\tau_{p_2}^2) + a_{p_2}\tau_{p_2}(1 + \omega^2\tau_{p_1}^2) \\ Z_p &= a_{p_1}\tau_{p_1}^2(1 + \omega^2\tau_{p_2}^2) + a_{p_2}\tau_{p_2}^2(1 + \omega^2\tau_{p_1}^2) \end{aligned} \tag{18}$$

(2) The reference contains a scatterer and the sample contains the dye. For $a = a_2/a_1$ we obtain

$$\tan \Phi = \omega \frac{\tau_1^2(1 + \omega^2\tau_2^2) + a\tau_2^2(1 + \omega^2\tau_1^2)}{\tau_1(1 + \omega^2\tau_2^2) + a\tau_2(1 + \omega^2\tau_1^2)} \tag{19}$$

The first- and second-order derivatives of eqn. (19) can easily be given explicitly. Therefore this formula is very convenient for use in a least-squares procedure.

If rotational diffusion is included, eqns. (16) and (17) are still valid but care must be taken with the interpretation of τ_i and a_i. The impulse response for parallel and vertically polarized emission for the simplest case of a rotating sphere and single-exponential luminescence decay is given by [20]

$$\alpha = \begin{cases} 4/5 & \text{for parallel polarization} \\ -2/5 & \text{for vertical polarization} \end{cases} \tag{20}$$

If we substitute

$$\tau = \tau_1 \quad \text{and} \quad \frac{1}{\tau_1} + \frac{1}{\tau_{\text{rot}}} = \frac{1}{\tau_2} \tag{21}$$

eqn. (19) can be applied which, after some rearrangement, leads to

$$\tan \Phi = \omega \frac{(1/\tau + 1/\tau_{\text{rot}})^2 + \omega^2 + \alpha(1/\tau^2 + \omega^2)}{(1/\tau)\{(1/\tau + 1/\tau_{\text{rot}})^2 + \omega^2\} + \alpha(1/\tau + 1/\tau_{\text{rot}})(1/\tau^2 + \omega^2)} \tag{22}$$

A special experimental situation exists if the sample and the reference compartment contain the same dye but the emission is observed at different polarizations. This case has been discussed by Weber [21]. Inserting eqn. (21) into eqn. (16) gives the following equation:

$$\tan(\Phi_S - \Phi_R) = \pm\omega \frac{\tau}{(9/10)(\tau_{\text{rot}}/\tau + \omega^2\tau\tau_{\text{rot}}) + (5/6)(\tau/\tau_{\text{rot}}) + 2} \tag{23}$$

This formula is equivalent to eqn. (25) of ref. 21 but is more convenient for our purposes. The plus sign applies if the sample is observed at parallel polarization and the reference is observed at vertical polarization.

It follows from eqn. (23) that the phase shifts observed in such an experiment contain the rotational relaxation constant as well as the excited state lifetime. These parameters can be evaluated in two ways.

(1) τ is measured independently as the phase shift between the sample under magic angle polarization and a scatterer. τ_{rot} is then easily and accurately calculated from the analytical solution of eqn. (23). An error analysis shows that the value of τ_{rot} is insensitive to errors in τ. The data in Table 4 were obtained in this way.

(2) τ and τ_{rot} are jointly determined by application of non-linear least-squares methods to eqn. (23). By careful investigation of the geometry of the χ^2 surface in parameter space it is possible to identify those domains where the procedure is applicable. It is found that contours of constant χ^2 are elliptical in the proximity of the χ^2 minimum if both τ and τ_{rot} are greater than 4 ns, which indicates that eqn. (23) is approximately linear in these parameters. In this case the standard deviations σ_τ and $\sigma_{\tau_{rot}}$ can be calculated as the square root of the diagonal elements of the variance–covariance matrix of the parameters [22]. The σ values calculated in this way for τ, $\tau_{rot} < 4$ ns are only approximate and tend to lose their meaning as soon as either of the parameters falls below 1 ns; τ and τ_{rot} are then strongly correlated, the χ^2 surface is very flat and the contours are elongated and not elliptical. The two parameters cannot be determined simultaneously in such situations.

The relative standard deviations $\sigma_\tau{}^r$ and $\sigma_{\tau_{rot}}{}^r$ are shown in Figs. 4(a) and 4(b) respectively as contours in the (τ, τ_{rot}) plane for simulated data (seven Φ values between 20 and 50 MHz with σ_Φ = 1 mrad):

$$\sigma_{\tau_i}{}^r = \frac{\sigma_{\tau_i}}{\tau_i} \times 100 \qquad (24)$$

The topography of these two figures confirms the above qualitative statements: towards the left and lower edges of the parameter plane neither of the parameters can be fitted with acceptable confidence, whereas they are well determined everywhere else. It must be remembered that these findings are specific to the chosen frequency range.

In a previous paper in this series [7] we proposed two methods for solving the problem of the wavelength-dependent instrumental response Δt_{inst}. The first could not be applied since no dye has yet been found whose decay is wavelength independent within the accuracy of our experiments. The preliminary data given in Table 1 of ref. 7 contain the instrumental delay together with a small change in the lifetime of rhodamine 6G. The second method should provide accurate information about Δt_{inst} if the lifetime τ of the dye is long (greater than 20 ns).

Two additional absolute calibration methods which do not rely on any assumptions concerning the decay of dyes are as follows.

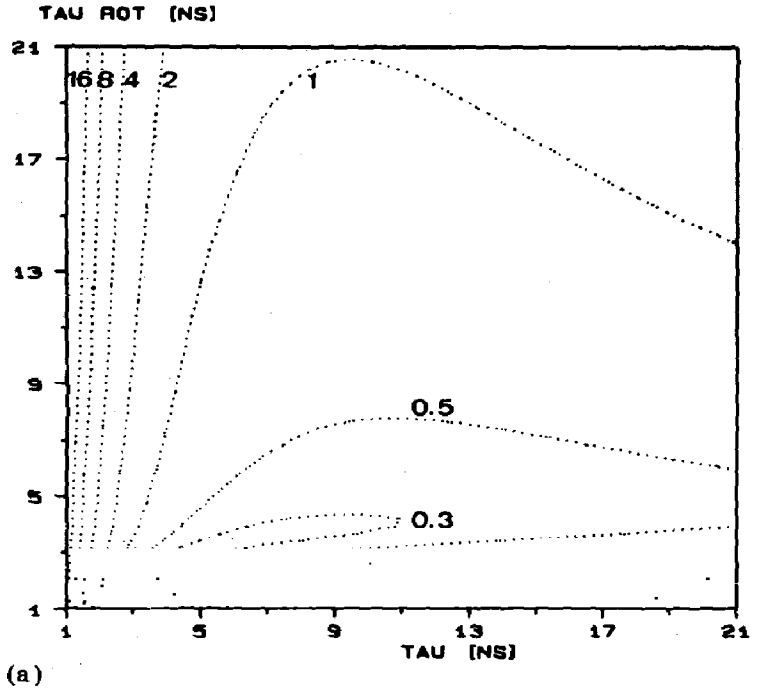

(a)

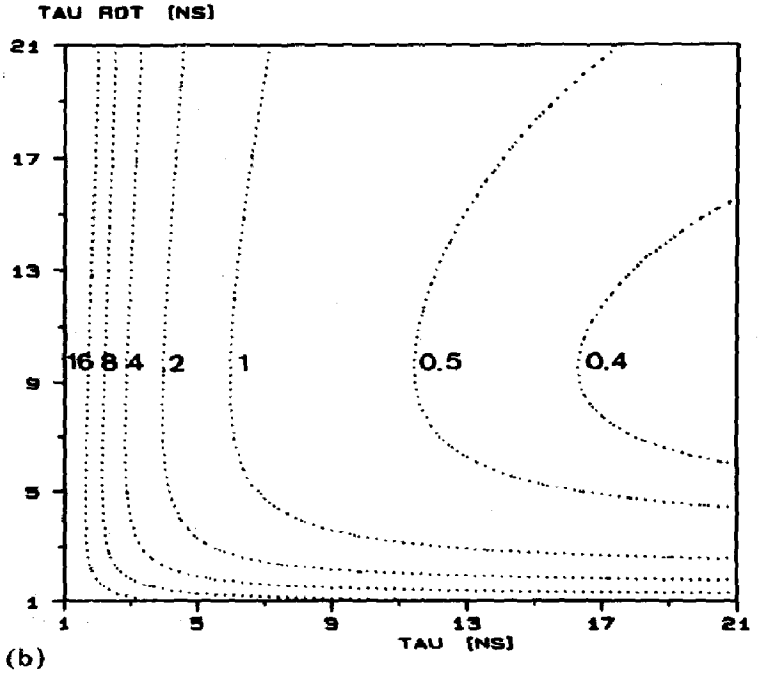

(b)

Fig. 4. Relative standard deviations (a) $\sigma_\tau{}^r$ and (b) $\sigma_\tau{}^r{}_{rot}$ in per cent obtained from a least-squares fit of eqn. (23) to simulated data.

TABLE 5

Influence of the instrumental delay on the determination of single-exponential lifetimes

Dye	*Raw data*		*Corrected for instrumental delay*	
	τ (ns)	Red χ^2	τ (ns)	Red χ^2
Fluorescein (EtOH–10^{-3} M NaOH)	4.205	2.76	4.126	0.80
Fluorescein ethyl ester (EtOH–10^{-3} M NaOH)	4.528	4.77	4.441	1.23
Coumarin 535 (EtOH)	2.857	0.28	2.794	0.08

Excitation, 482.5 nm; emission, 535 nm; polarization, magic angle; frequency range, seven values between 20 and 50 MHz; Δt_{inst} = 43.3 ps.

(1) The use of Raman lines [23].

(2) Simultaneous modulation of two different lines (λ_1, λ_2) of the same laser beam which allows the determination of Δt_{inst} between λ_1 and λ_2. The exciting light is scattered and the two wavelengths are selected by two monochromators. The delay for the 482.5 nm and 530.9 nm lines of our Kr^+ laser is measured as 40 ± 2 ps for an RCA C31024 photomultiplier at −2000 V. This value was used to correct all measurements; it was assumed that the delay was frequency independent and varied linearly with the wavelength difference.

Table 5 shows the influence of Δt_{inst} on the determination of a single-exponential lifetime. A significant reduction of χ^2 is obtained when the data are corrected for this delay.

One final remark concerning the goodness of fit criterion red χ^2 which appears in Tables 1 - 3 and 5 seems appropriate. This statistic, which measures the discrepancy between the residuals of the fit and the estimated variances of the data, should lie close to unity for a correct model function and follow the χ^2 distribution [24]. However, the reduced χ^2 values of the best fits to our data are generally much less than unity. This means that the variances $\sigma_\Phi{}^2$ of the measured phase shifts, which are calculated according to the error analysis outlined in earlier papers in this series [5, 8], overestimate the effective uncertainty of the data which indicates that the accuracy of our measurements is even better than that previously reported [8].

5. Conclusions

It has long been known that modulation techniques are basically very powerful methods of obtaining high quality kinetic information [18, 25]. The major drawback in fluorescence decay analysis up to the present time

has been its inability to resolve non-single-exponential kinetics. The technical problems are now solved. This opens a broad field of applications extending the range of the many interesting single-photon-counting studies.

To our surprise rhodamine 6G and coumarin 535 in glycerol show far more complex decay kinetics than has been assumed up to now. A possible interpretation is given in terms of various conformations which are stabilized by the highly viscous solvent. This is supported by the exact single-exponential behaviour of coumarin 535 in ethanol. Many more data are needed to confirm and refine this picture. Nevertheless we have succeeded in advancing into the fascinating excited state behaviour of large molecules in solution.

Acknowledgment

We should like to thank the Swiss National Science Foundation (Grant 2.901-0.83) for financial support.

References

1 G. Calzaferri, H. Gugger and S. Leutwyler, *Helv. Chim. Acta, 59* (1976) 1969.
2 H. Güsten and R. Meisner, *J. Photochem., 21* (1983) 53.
D. J. Cowley and I. Pasha, *J. Chem. Soc., Perkin Trans. II*, (1981) 918.
H. Takemoto, S. Inoue, T. Yasunaga, M. Sukigara and Y. Toyoshima, *J. Phys. Chem., 85* (1981) 1032.
D. Cremers and M. W. Windsor, *Chem. Phys. Lett., 71* (1980) 27.
R. Griebel, *Ber. Bunsenges. Phys. Chem., 84* (1980) 84.
K. Onuki, K. Kurihara, Y. Toyoshima and M. Sukigara, *Bull. Chem. Soc. Jpn., 53* (1980) 1914.
J. Jansen and W. Lüttke, *J. Mol. Struct., 81* (1982) 207.
3 E. M. Kosower, *Acc. Chem. Res., 15* (1982) 259.
4 S. K. Chakrabarti and W. R. Ware, *J. Chem. Phys., 55* (1971) 5494.
K. Egawa, N. Nakashima, W. Mataga and Ch. Yamanaka, *Bull. Chem. Soc. Jpn., 44* (1971) 3287.
R. P. Detoma and L. Brand, *Chem. Phys. Lett., 47* (1977) 231.
E. D. Matayoshi and A. M. Kleinfeld, *Biochim. Biophys. Acta, 644* (1981) 233.
D. A. Barrow and B. R. Lentz, *Chem. Phys. Lett., 104* (1984) 163.
St. R. Meech and D. Phillips, *J. Photochem., 23* (1983) 193.
5 H. Gugger and G. Calzaferri, *J. Photochem., 13* (1980) 21, 295.
6 H. Gugger and G. Calzaferri, *J. Photochem., 16* (1981) 13.
7 J. Baumann and G. Calzaferri, *J. Photochem., 22* (1983) 297.
8 J. Baumann and G. Calzaferri, *J. Photochem., 23* (1983) 387.
9 J. Baumann, G. Calzaferri and Th. Hugentobler, *Chem. Phys. Lett.*, in the press.
10 M. M. Malley and G. Mourou, *Opt. Commun., 10* (1974) 329.
11 G. G. Guibault, *Practical Fluorescence*, Marcel Dekker, New York, 1973, p. 293.
12 R. Hoffmann, *J. Chem. Phys., 39* (1963) 1397.
R. Hoffmann and W. N. Lipscomb, *J. Chem. Phys., 36* (1962) 2179, 3489; *37* (1962) 2872.
13 R. Pariser and R. G. Parr, *J. Chem. Phys., 21* (1953) 466, 767.
N. Mataga and K. Nishimoto, *Z. Phys. Chem. N.F., 13* (1957) 140.
14 F. A. Cotton, *Chemical Applications of Group Theory*, Wiley-Interscience, New York, 2nd edn., 1971, p. 168.

15 R. S. Mulliken, *J. Chem. Phys.*, *23* (1955) 1833.
G. Calzaferri and F. Felix, *Helv. Chim. Acta*, *60* (1977) 730.
16 K. Fukui and H. Fujimoto, *Bull. Chem. Soc. Jpn.*, *41* (1968) 1989; *42* (1969) 3399.
R. F. Hudson, *Angew. Chem.*, *85* (1973) 63.
G. Klopman, *J. Am. Chem. Soc.*, *90* (1968) 223.
17 S. L. Shapiro and K. R. Winn, *Chem. Phys. Lett.*, *71* (1980) 440.
18 M. Eigen and L. DeMaeyer, in G. G. Hammes (ed.), *Techniques of Chemistry*, Vol. 4, Wiley, New York, 1974.
G. Weber, *J. Phys. Chem.*, *85* (1981) 949.
J. R. Lakowicz and A. Balter, *Photochem. Photobiol.*, *36* (1982) 125.
J. B. Birks and I. H. Munro, *Prog. React. Kinet.*, *4* (1967) 239.
H. P. Haar, U. K. A. Klein, F. W. Hafner and M. Hauser, *Chem. Phys. Lett.*, *49* (1977) 5633.
19 M. Schwartz, *Information, Transmission, Modulation and Noise*, McGraw-Hill, Tokyo, 1970.
20 T. Tao, *Biopolymers*, *8* (1969) 609.
21 G. Weber, *J. Chem. Phys.*, *66* (1977) 4081.
22 N. R. Draper and H. Smith, *Applied Regression Analysis*, Wiley, New York, 1966.
23 Sh. Kinoshita and T. Kushida, *Rev. Sci. Instrum.*, *53* (1982) 469.
24 P. R. Bevington, *Data Reduction and Error Analysis for the Physical Sciences*, McGraw-Hill, New York, 1969.
25 L. F. Phillips, *Prog. React. Kinet.*, *7* (1973) 84.